Optical Control of L-Type Ca^{2+} Channels Using a Diltiazem Photoswitch

Timm Fehrentz[1,15]*, Florian M.E. Huber[2,3,15], Nina Hartrampf[2], Tobias Bruegmann[4,5], James A. Frank[2,6], Nicholas H.F. Fine[7,8], Daniela Malan[4], Johann G. Danzl[9,10], Denis B. Tikhonov[11], Martin Sumser[2], Philipp Sasse[4], David J. Hodson[7,8], Boris S. Zhorov[11,12,13], Nikolaj Klöcker[1]*, and Dirk Trauner[2,14]*

[1] Institute of Neural and Sensory Physiology, Medical Faculty, University of Düsseldorf, 40225 Düsseldorf, Germany

[2] Department of Chemistry, University of Munich and Center for Integrated Protein Science (CIPSM), 81377 Munich, Germany

[3] Roche Diagnostics GmbH, DXRERA, 82377 Penzberg, Germany, present address

[4] Institute of Physiology I, Medical Faculty, University of Bonn, 53105 Bonn, Germany

[5] Research Training Group 1873, University of Bonn, 53105 Bonn, Germany

[6] Research Laboratory of Electronics, Massachusetts Institute of Technology, 50 Vassar St., Cambridge, MA 02139, USA, present address

[7] Institute of Metabolism and Systems Research (IMSR) and Centre of Membrane Proteins and Receptors (COMPARE), University of Birmingham, Birmingham B15 2TT, UK

[8] Centre for Endocrinology, Diabetes and Metabolism, Birmingham Health Partners, Birmingham, B15 2TH, UK.

[9] Department of NanoBiophotonics, Max Planck Institute for Biophysical Chemistry, 37077 Göttingen, Germany.

[10] Institute of Science and Technology Austria, 3400 Klosterneuburg, Austria, present address

[11] Sechenov Institute of Evolutionary Physiology and Biochemistry, Russian Academy of Sciences, 194356 St. Petersburg, Russia

[12] Institute of Molecular Biology and Genetics, Almazov Federal Heart, Blood and Endocrinology Centre, 197341, St. Petersburg, Russia

[13] Department of Biochemistry & Biomedical Sciences, McMaster University, Hamilton, L8S4K1 Canada

[14] Department of Chemistry and Neuroscience Institute, New York University, New York, NY 10012, U.S.A.

[15] These authors contributed equally to this work.

* correspondence to:

timm.fehrentz@gmail.com

nikolaj.klöcker@uni-duesseldorf.de

dirktrauner@nyu.edu

L-type Ca^{2+} channels (LTCCs) play a crucial role in excitation-contraction coupling and the release of hormones from secretory cells. They are targets of numerous antihypertensive and antiarrhythmic drugs such as diltiazem. Here, we present a photoswitchable derivative of diltiazem, FHU-779, which can be used to reversibly block endogenous LTCCs by light. FHU-779 is almost as potent as diltiazem itself, and can be used to place pancreatic β cell function and cardiac activity under optical control.

L-type Ca^{2+} channels (LTCCs, Ca_V1) serve fundamental physiological roles in excitable tissues[1]. Activated by membrane depolarization, LTCCs permit Ca^{2+} influx into cells and are key players in voltage-dependent signal transduction[1,2]. For instance, LTCCs are crucial for pacemaking, electrical conduction, and excitation-contraction coupling in the heart[1]. In pancreatic β cells, LTCCs are essential for excitation-secretion coupling affording insulin release[3]. To study the role of LTCCs in more detail, Ca^{2+} imaging techniques have been applied for monitoring the cytosolic Ca^{2+} concentration in living cells with high resolution[4,5]. However, tools to control Ca^{2+} influx through endogenous LTCCs with comparable temporal and spatial resolution have been lacking so far. We have addressed this experimental need by creating a photoswitch that enables control of LTCCs using light.

Based on the structure of the benzothiazepine-like Ca^{2+} channel blocker diltiazem, we synthesized the doubly-charged, hydrophilic photoswitch FHU-779 by installing a photoresponsive azobenzene moiety (**Fig. 1a**,**b**; for synthesis see **Supplementary Note**). Under blue (470 nm) illumination or in the dark, the compound rests in its thermally more stable *trans*-state. Upon UV-A irradiation (385 nm), the compound is reversibly converted into its energetically elevated *cis*-state, which has a bent conformation. We characterized the spectral properties of *cis*- and *trans*-FHU-779 by UV-Vis spectroscopy (**Fig. 1c**). Thermal relaxation from *cis*- to *trans*-FHU-779 detected at 360 nm followed a mono-exponential time course with a time constant of $\tau = 4081 \pm 71$ min (**Supplementary Fig. 1**). To determine whether FHU-779 was able to afford optical control of LTCC function, we performed whole-cell patch clamp recordings using HEK293T cells heterologously expressing Ca_V1 channels. Current-voltage (I-V) relationships for $Ca_V1.2$ and $Ca_V1.3$ in the

presence of *cis*- and *trans*-FHU-779 are shown in **Fig. 1d** and **Supplementary Fig. 2**, respectively (n = 3 cells each). In its *trans*-state, FHU-779 strongly reduced inward currents conducted by both channel subtypes. The block of Ca_v1 channels was reversible when FHU-779 was repeatedly photoswitched between its *trans*- and *cis*-states (**Fig. 1e,f**; **Supplementary Fig. 2**). Quantification of block induced by 25 µM externally applied FHU-779 was impeded by LTCC current rundown[6], yielding photoswitching efficacies of 46.5 ± 7.6% and 46.4 ± 5.4% for $Ca_v1.2$ (n = 10 cells) and $Ca_v1.3$ channels (n = 9 cells), respectively (**Fig. 1g**). In contrast, FHU-779-mediated photoswitching of voltage-gated potassium (K_v) channels, which are reportedly blocked by high dose diltiazem[7], was far less efficient with only 6.2 ± 2.7% (n = 6 cells) and 5.9 ± 3.0% (n = 6 cells) photoswitching detected for heterologously expressed Shaker-IR or K_v channels, respectively. Also, photoswitching quantification against voltage-gated sodium channel $Na_v1.5$ by FHU-779 showed only 5.4 ± 0.9% change (n = 10 cells). These data demonstrate that FHU-779 endows light sensitivity to the two major LTCC subtypes, $Ca_v1.2$ and $Ca_v1.3$, but has negligible effects on K_v and Na_v channels. In an attempt to determine the access route of FHU-779 into LTCCs, the drug was applied intracellularly via the patch pipette. Whole-cell dialysis of 100 µM FHU-779 resulted in negligible photoswitching of both $Ca_v1.2$ (8.6 ± 6.0%; n = 4 cells) and $Ca_v1.3$ currents (2.0 ± 4.6%; n = 7 cells, **Fig. 1g**). This result suggests that FHU-779 enters LTCCs from the extracellular side rather than from the cytosol[8].

To more precisely quantify FHU-779 photoswitching, we loaded HEK293T cells heterologously expressing a $Ca_v1.2$ mutant deficient for channel inactivation ($Ca_v1.2\Delta1671$)[9] with the fluorescent Ca^{2+} indicator Fura-2 and performed ratiometric Ca^{2+} imaging[10]. LTCC channels were activated by membrane depolarization with high extracellular [K^+], and the consecutive increase in intracellular Ca^{2+} ($[Ca^{2+}]_i$) was recorded (**Fig. 2a**; **Supplementary Fig. 3; Supplementary Movies 1-3** and online methods). Subsequent wash-in of FHU-779 decreased cytosolic Ca^{2+} levels in the dark, whereas changing illumination wavelengths between 480 nm and 380 nm allowed for reliable optical control of Ca^{2+} influx into cells.

The Ca^{2+} imaging based quantification of $Ca_v1.2$ block by diltiazem yielded a dose-response relationship with an IC_{50} of 2.7 µM ± 1.0% (**Supplementary Fig. 3**), which is in accordance with the literature[11,12] and in the same range as *trans*-FHU-779 showing an IC_{50} of 8.3 µM ± 0.6% (**Fig. 2b**). The difference between both dose-response relationships

of *trans*-FHU-779 and *cis*-FHU-779 data represents quantitative photoswitching amplitudes at a given concentration.

To rationalize these results, we constructed an open-state $Ca_V1.2$ model and docked FHU-779 using a previously elaborated approach[13] with the open Na_VAb channel X-ray structure as a template[14] (**Fig. 2c**,**d**; **Supplementary Fig. 4**,**5**; **Supplementary Table 1**,**2**; online methods). The model accommodated *trans*-FHU-779 with the tricyclic moiety and the long chain as predicted for benziazem[15], which shares a similar chemical structure as FHU-779. The benzothiazepine moiety was bound in the repeat III/IV fenestration, the protonated nitrogen resided near the selectivity filter, and the long photoswitchable moiety extended along the inner pore (**Fig. 2c**). *cis*-FHU-779 was also accommodated in the inner cavity, but the folded conformation was too bulky to access this site either through the open activation gate or a fenestration (**Fig. 2d**).

To further explore the application spectrum of FHU-779 in primary cells and tissue endogenously expressing LTCCs, we used pancreatic islets and monitored $[Ca^{2+}]_i$ in β cells by Fluo-8 fluorescence intensity imaging (**Fig. 3a**). When triggered by LTCC-mediated Ca^{2+} influx, pancreatic β cells secrete insulin to regulate blood glucose levels[16]. First, the sulfonylurea and ATP-sensitive K^+ channel (K_{ATP}) blocker tolbutamide was applied to depolarize β cells and fully activate LTCCs[17]. This led to Ca^{2+} influx that was strongly reduced by *trans*-FHU-779 when cells were illuminated at 470 nm (**Fig. 3a**). This effect was reversed by illumination at 395 nm, yielding 52.2 ± 2.7% photoswitching (n = 9 islets, see online methods). Controls were performed relative to the magnitude of tolbutamide alone, and with diltiazem- and tolbutamide-treated islets (n = 9, **Supplementary Fig. 6**). Prior application of a saturating concentration of diltiazem precluded photoswitching by FHU-779 (**Supplementary Fig. 6**). Whole-cell patch clamp experiments in dissociated pancreatic β cells displayed reduced inward currents through LTCCs at 470 nm as compared to 370 nm light in the presence of FHU-779 (**Fig. 3b**), reinforcing our imaging results. In the absence of FHU-779, corresponding I-V relationships did not differ in current amplitude in response to illumination (**Supplementary Fig. 6**). Insulin secretion was determined in islets under control conditions (tolbutamide), or following application of diltiazem and *cis*- or *trans*-FHU-779 (**Fig. 3c**). As expected, only diltiazem and *trans*-FHU-779 application were able to significantly reduce insulin secretion. To demonstrate the spatiotemporal control of LTCCs, we reversibly photoactivated FHU-779 in a single

from a doublet or triplet islets of Langerhans (**Supplementary Fig. 7**), as well as in single beta cells residing within the intact microorgan (**Fig. 3d-f**), while performing Ca^{2+} imaging. As such, FHU-779 enables robust and precise spatiotemporal optical control of endogenous LTCC function, Ca^{2+} fluxes and insulin secretion in pancreatic β cells.

FHU-779 was also applicable to explanted hearts perfused in the Langendorff configuration. Besides coupling excitation and contraction in cardiomyocytes, LTCCs are important for sinoatrial pacemaking in the right atrium and atrioventricular conduction[1]. FHU-779 was perfused into coronary arteries and the right atrium was illuminated. In line with the LTCC-block by *trans*-FHU-779, illumination with 480 nm reduced heart rate, which was quickly reversed by 380 nm illumination (**Fig. 3g**). Photoswitching significantly affected the heart rate by 5.8 ± 1.8% (n = 4 hearts) in comparison to control experiments, which were performed prior to FHU-779 application but with the same illumination protocol (**Fig. 3h**). We also screened for the optimal irradiation wavelength, and found that 360 nm illumination achieved the largest increase in heart rate while 400 nm light was still effective (**Supplementary Fig. 8**). Furthermore, we analyzed the relationship between cycle length for switching between 480 nm and 380 nm illumination and heart rate response and found a maximal effect at 30 s of illumination (**Supplementary Fig. 8**). These experiments were further substantiated by whole-cell patch-clamp recordings of LTCC currents from adult cardiomyocytes and revealed photoswitching of 20.5 ± 8.8% (n = 12 cells) (**Supplementary Fig. 8**). To demonstrate spatial control of cardiomyocyte function, Cor4U cardiomyocytes were plated on microelectrode arrays (MEA) and treated with FHU-779. The duration of extracellular field potentials (FPs), which is reflecting the LTCC-dependent plateau phase of the cardiac action potential[18] was measured from individual electrodes, and only part of the MEA was illuminated with either 385 nm or 480 nm light. The illuminated electrodes showed a FP prolongation upon UV-light and FP shortening using 480 nm indicating activation and block of LTCCs, respectively (**Fig. 3i**). This effect could be changed repetitively and was not observed on non-illuminated electrodes of the same MEA (**Supplementary Fig. 9**).

In conclusion, we present a tool to reversibly control one of the main gates of Ca^{2+} influx into excitable cells, the LTCCs, at spatiotemporal precision of light. Derived from the clinically used LTCC blocker diltiazem, our molecule is applicable in dissociated primary

cells and *ex vivo* organ preparations. In contrast to genetically encoded optogenetic tools, such as ChR2[19], OptoSTIM1[20], or Opto-CRACK[20], FHU-779 bestows light sensitivity to *endogenous* LTCCs. Compared to light-flash photolysis of nifedipine for optical control of LTCC activity[21,22], FHU-799 extends experimental options by adding a high temporal reversibility. Thus, biological processes involving LTCC-related Ca^{2+}oscillations may now be accessed; also, localized modulation of LTCC-induced cardiac arrhythmia can be envisaged. Since FHU-779 serves as new lead structure, further chemical modifications will multiply specific LTCC tools and thus biological applications.

Author contribution:

The project was conceived by T.F., N.K. and D.T.. Patch clamp characterization of FHU-779 was carried out by T.F., J.F., D.M., T.B. and J.G.D.. Ratiometric Ca^{2+} imaging in HEK293T cells was performed by T.F. and M.S.. Ca^{2+} imaging of pancreatic islets was carried out by N.H.F.F and D.J.H.. Heart rate modulation on Langendorff-perfused hearts was performed by T.B., T.F. and P.S. and FP experiments by D.M. and P.S.. Molecular modeling was performed by D.B.T. and B.S.Z.. Synthesis of FHU-779 was carried out by F.M.E.H. and N.H.. T.F., D.T. and N.K. wrote the manuscript with contributions from all authors.

Acknowledgements:

We would like to thank Gary R. Lewin and Mirko Moroni (MDC Berlin) for the TRAAK-GFP construct, Manu Ben Johnny (Johns Hopkins University) for $Ca_v1.2\Delta1671$ construct and Jörg Striessnig (University of Innsbruck) for $Ca_v1.3$, $Ca_v1.2$, β_3, $\alpha_2\delta$ constructs. T.F. and J.G.D thank Stefan Walter Hell for general support. D.T. was supported by the Deutsche Forschungsgemeinschaft (SFB 749) and Center for Integrated Protein Science Munich (CIPSM). M.S. was supported by the DFG (SPP1926). N.K. receives support from the DFG (SFB 1116, TP A01) and the BMBF (DZHK, FKZ: 81X2800159). D.J.H. was supported by a Diabetes UK R.D. Lawrence (12/0004431) and EFSD/Novo Nordisk Rising Star Fellowships, a Wellcome Trust Institutional Support Award, and COMPARE Primer, MRC Project (MR/N00275X/1) and ERC Starting Grants (OptoBETA; 715884). N.V. thanks the "Deutsche Telekom Stiftung" and the LMUMentoring program for financial support. B.S.Z. acknowledges grants from NSERC, Canada (GRPIN-2014-04894) and Russian Science Foundation (17-15-01292). P.S. was supported by the Deutsche Forschungsgemeinschaft (DFG, German Research Foundation, GRK1873, SA 1785/7-1, SA 1785/9-1).

1. Zamponi, G.W., Striessnig, J., Koschak, A. & Dolphin, A.C. The Physiology, Pathology, and Pharmacology of Voltage-Gated Calcium Channels and Their Future Therapeutic Potential. *Pharmacol. Rev.* **67**, 821-70 (2015).
2. Catterall, W.A., Wisedchaisri, G. & Zheng, N. The chemical basis for electrical signaling. *Nat. Chem. Biol.* **13**, 455-463 (2017).
3. Wheeler, D.G., Barrett, C.F., Groth, R.D., Safa, P. & Tsien, R.W. CaMKII locally encodes L-type channel activity to signal to nuclear CREB in excitation-transcription coupling. *J. Cell. Biol.* **183**, 849-63 (2008).

4. Tour, O. et al. Calcium Green FlAsH as a genetically targeted small-molecule calcium indicator. *Nat. Chem. Biol.* **3**, 423-31 (2007).
5. Grienberger, C. & Konnerth, A. Imaging calcium in neurons. *Neuron* **73**, 862-85 (2012).
6. Kepplinger K.J.F., R.C. The run-down phenomenon. *voltage-gated calcium channels*, 219-230 (2005).
7. Grissmer, S. et al. Pharmacological characterization of five cloned voltage-gated K+ channels, types Kv1.1, 1.2, 1.3, 1.5, and 3.1, stably expressed in mammalian cell lines. *Mol. Pharmacol.* **45**, 1227-34 (1994).
8. Shabbir, W. et al. Interaction of diltiazem with an intracellularly accessible binding site on Ca(V)1.2. *Br. J. Pharmacol.* **162**, 1074-82 (2011).
9. Mori, M.X., Erickson, M.G. & Yue, D.T. Functional stoichiometry and local enrichment of calmodulin interacting with Ca2+ channels. *Science* **304**, 432-5 (2004).
10. Grynkiewicz, G., Poenie, M. & Tsien, R.Y. A new generation of Ca2+ indicators with greatly improved fluorescence properties. *J. Biol. Chem.* **260**, 3440-50 (1985).
11. Freedman, S.B., Dawson, G., Villereal, M.L. & Miller, R.J. Identification and characterization of voltage-sensitive calcium channels in neuronal clonal cell lines. *J. Neurosci.* **4**, 1453-67 (1984).
12. Hockerman, G.H., Dilmac, N., Scheuer, T. & Catterall, W.A. Molecular determinants of diltiazem block in domains IIIS6 and IVS6 of L-type Ca(2+) channels. *Mol. Pharmacol.* **58**, 1264-70 (2000).
13. Zhang, Y. et al. The Receptor Site and Mechanism of Action of Sodium Channel Blocker Insecticides. *J. Biol. Chem.* **291**, 20113-24 (2016).
14. Lenaeus, M.J. et al. Structures of closed and open states of a voltage-gated sodium channel. *Proc. Natl. Acad. Sci. U S A* **114**, E3051-E3060 (2017).
15. Tikhonov, D.B. & Zhorov, B.S. Molecular modeling of benzothiazepine binding in the L-type calcium channel. *J. Biol. Chem.* **283**, 17594-604 (2008).
16. Rutter, G.A., Pullen, T.J., Hodson, D.J. & Martinez-Sanchez, A. Pancreatic beta-cell identity, glucose sensing and the control of insulin secretion. *Biochem. J.* **466**, 203-18 (2015).
17. Cook, D.L. & Ikeuchi, M. Tolbutamide as mimic of glucose on beta-cell electrical activity. ATP-sensitive K+ channels as common pathway for both stimuli. *Diabetes* **38**, 416-21 (1989).
18. Lapp, H. et al. Frequency-dependent drug screening using optogenetic stimulation of human iPSC-derived cardiomyocytes. *Sci. Rep.* **7**, 9629 (2017).
19. Zhang, F., Aravanis, A.M., Adamantidis, A., de Lecea, L. & Deisseroth, K. Circuit-breakers: optical technologies for probing neural signals and systems. *Nat. Rev. Neurosci.* **8**, 577-81 (2007).
20. Ma, G. et al. Optogenetic toolkit for precise control of calcium signaling. *Cell Calcium* (2017).
21. Morad, M., Goldman, Y.E. & Trentham, D.R. Rapid photochemical inactivation of Ca2+-antagonists shows that Ca2+ entry directly activates contraction in frog heart. *Nature* **304**, 635-8 (1983).
22. Gurney, A.M. & Lester, H.A. Light-flash physiology with synthetic photosensitive compounds. *Physiol. Rev.* **67**, 583-617 (1987).

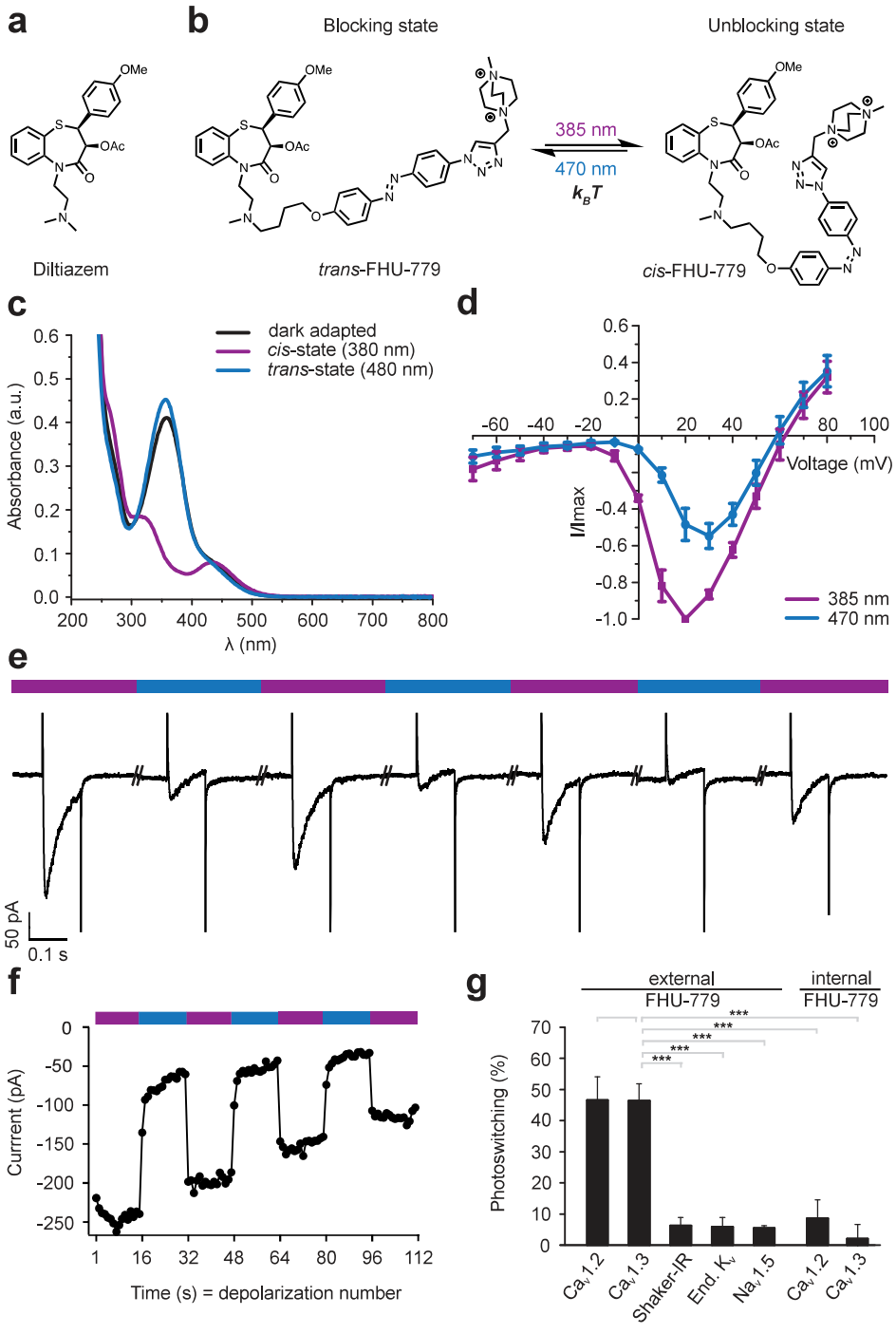
a
b
Blocking state
Unblocking state
385 nm
470 nm
k_BT
Diltiazem
trans-FHU-779
cis-FHU-779
c
dark adapted
cis-state (380 nm)
trans-state (480 nm)
Absorbance (a.u.)
λ (nm)
d
I/Imax
Voltage (mV)
385 nm
470 nm
e
50 pA
0.1 s
f
Current (pA)
Time (s) = depolarization number
g
external FHU-779
internal FHU-779
Photoswitching (%)
Cav1.2
Cav1.3
Shaker-IR
End. Kv
Nav1.5
Cav1.2
Cav1.3

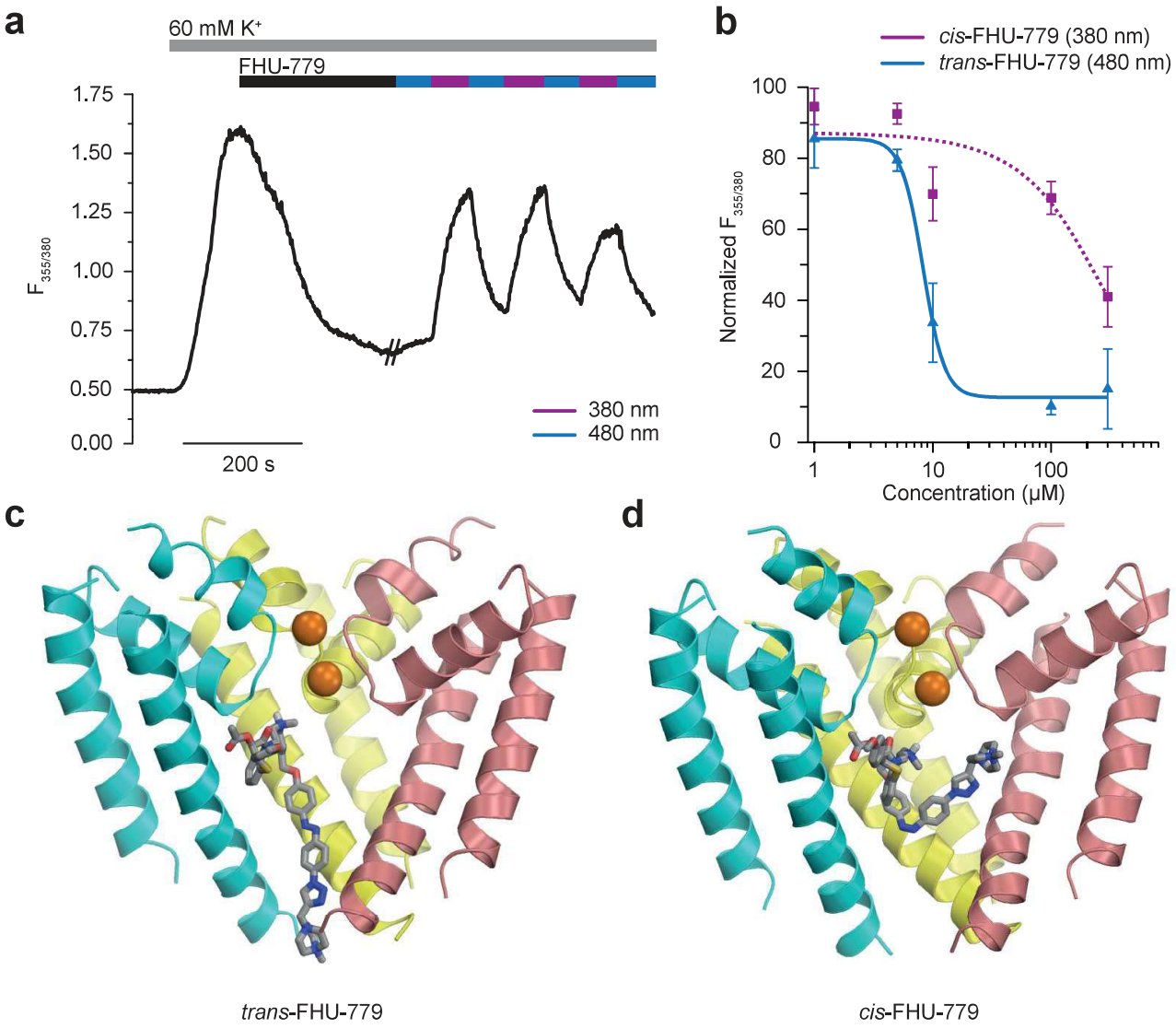

trans-FHU-779

cis-FHU-779

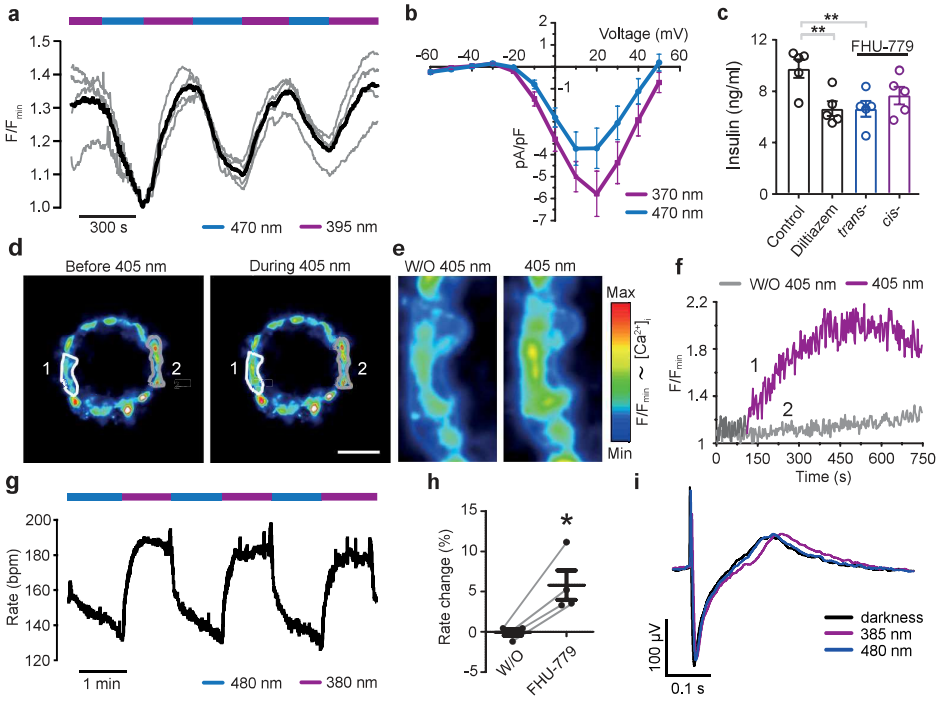
a
F/F$_{min}$
300 s
470 nm
395 nm
b
Voltage (mV)
pA/pF
370 nm
470 nm
c
FHU-779
Insulin (ng/ml)
Control
Diltiazem
trans-
cis-
d
Before 405 nm
During 405 nm
e
W/O 405 nm
405 nm
Max
Min
F/F$_{min}$ ~ [Ca^{2+}]$_i$
f
W/O 405 nm
405 nm
F/F$_{min}$
Time (s)
g
Rate (bpm)
1 min
480 nm
380 nm
h
Rate change (%)
W/O
FHU-779
i
darkness
385 nm
480 nm
100 µV
0.1 s

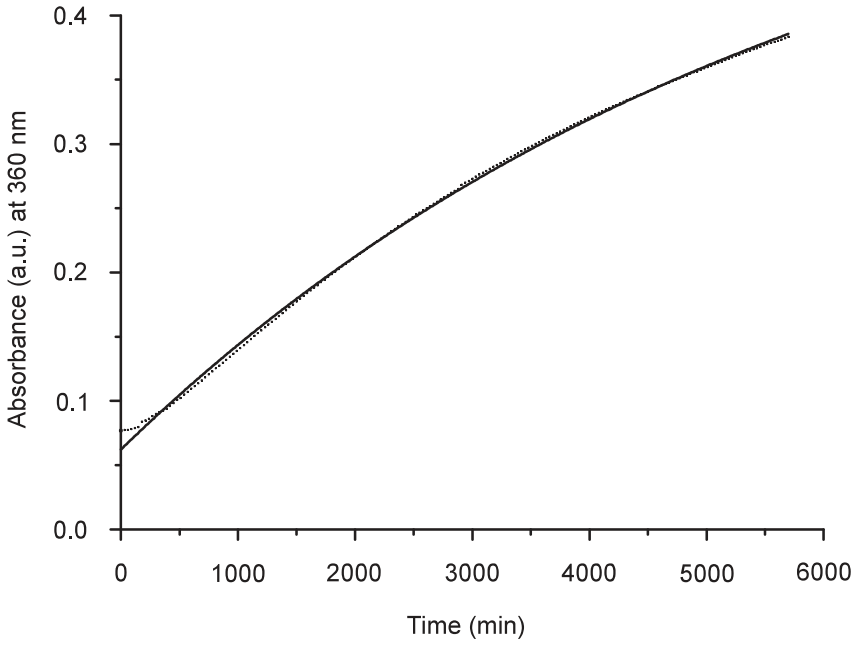
0.4
0.3
0.2
0.1
0.0
Absorbance (a.u.) at 360 nm
0
1000
2000
3000
4000
5000
6000
Time (min)

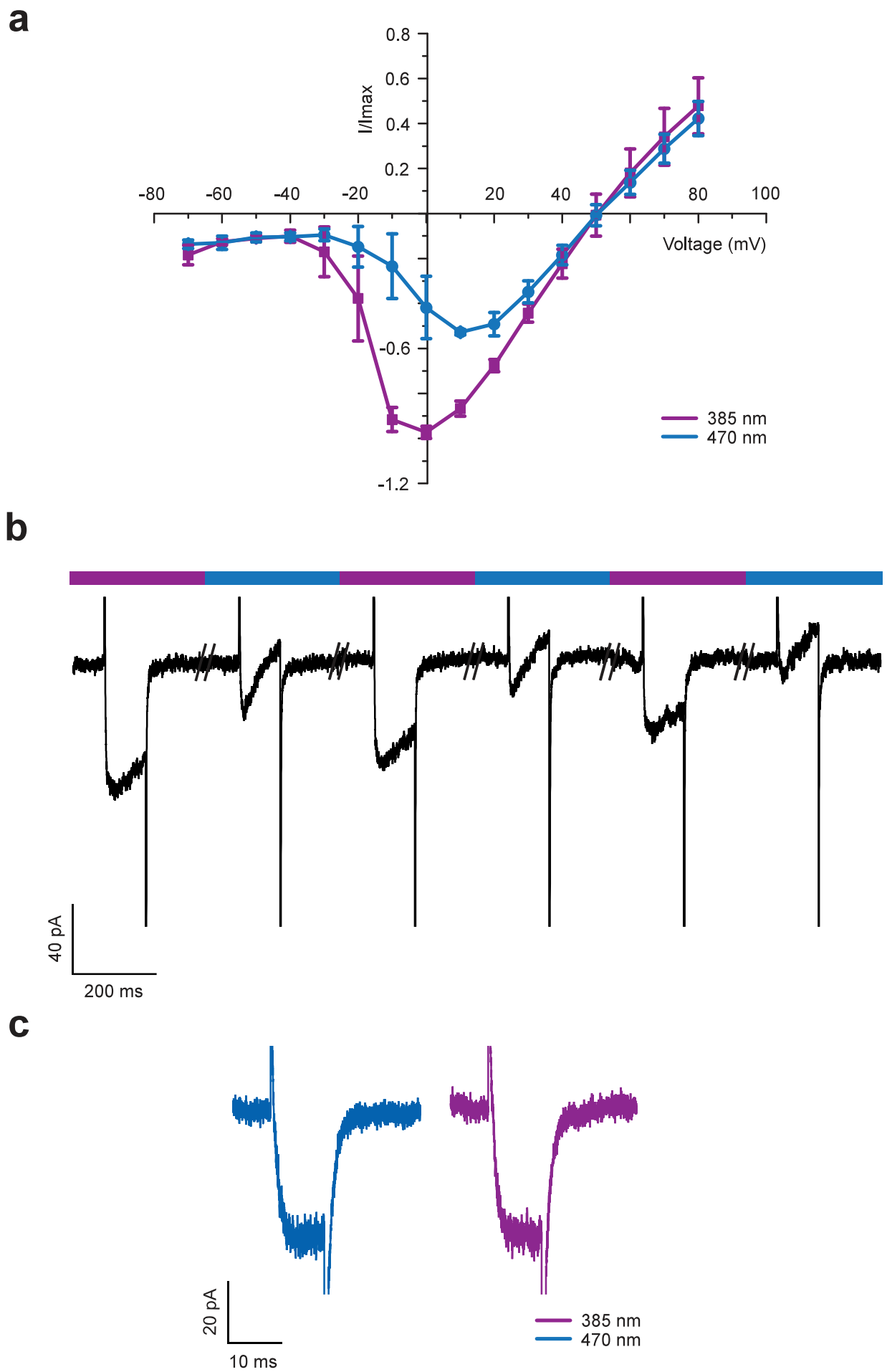
a
0.8
0.6
0.4
0.2
I/Imax
-80
-60
-40
-20
20
40
80
100
Voltage (mV)
-0.6
-1.2
385 nm
470 nm
b
40 pA
200 ms
c
20 pA
10 ms
385 nm
470 nm

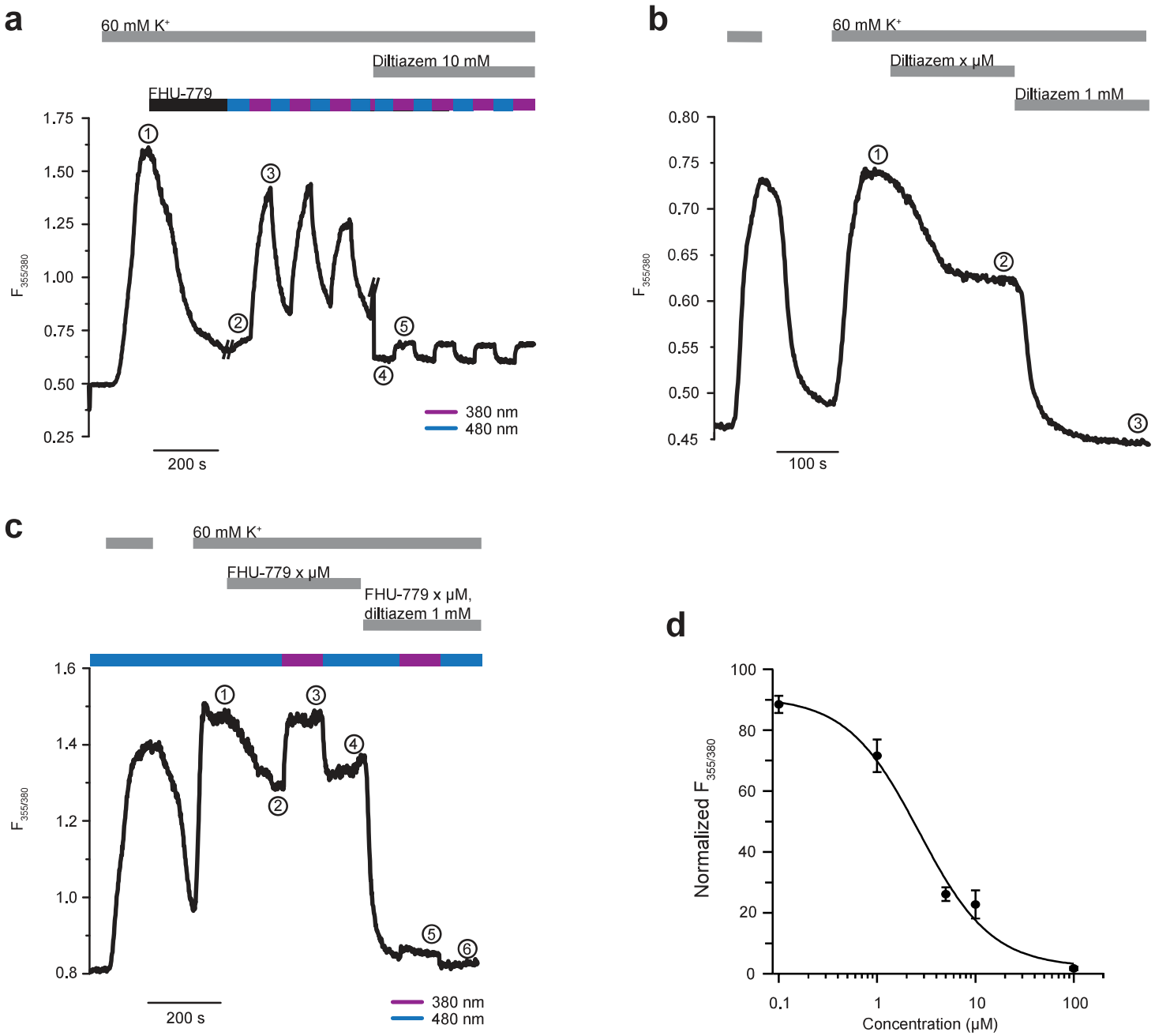
a
60 mM K+
Diltiazem 10 mM
FHU-779
1.75
1.50
1.25
1.00
0.75
0.50
0.25
F355/380
1
2
3
4
5
380 nm
480 nm
200 s
b
60 mM K+
Diltiazem x µM
Diltiazem 1 mM
0.80
0.75
0.70
0.65
0.60
0.55
0.50
0.45
F355/380
1
2
3
100 s
c
60 mM K+
FHU-779 x µM
FHU-779 x µM,
diltiazem 1 mM
1.6
1.4
1.2
1.0
0.8
F355/380
1
2
3
4
5
6
200 s
380 nm
480 nm
d
100
80
60
40
20
0
Normalized F355/380
0.1
1
10
100
Concentration (µM)

a

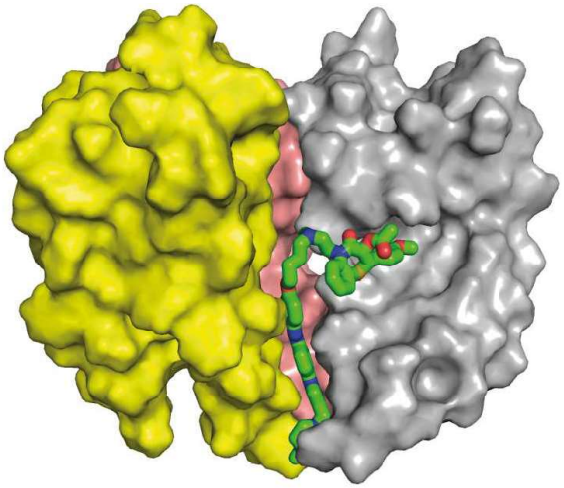

trans-FHU-779

b

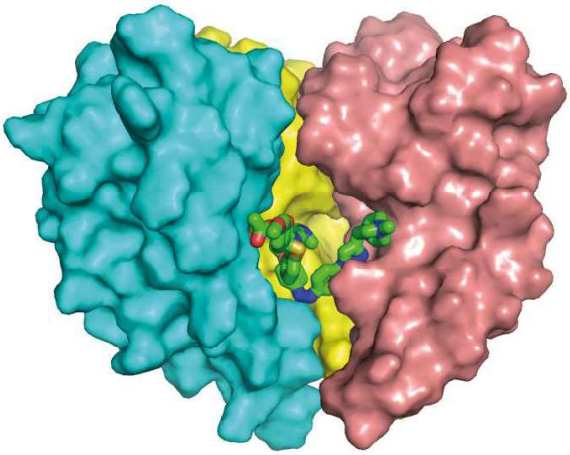

cis-FHU-779

a

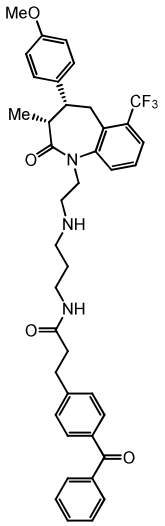

Benziazem derivative

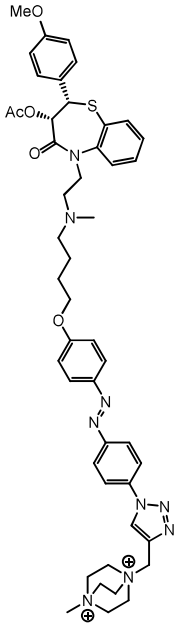

FHU-779

b

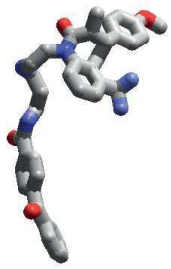

Benziazem derivative

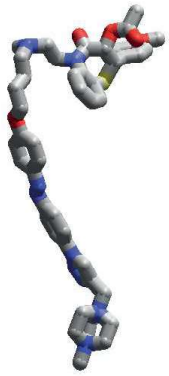

trans-FHU-779

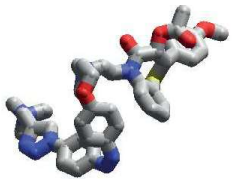

cis-FHU-779

c

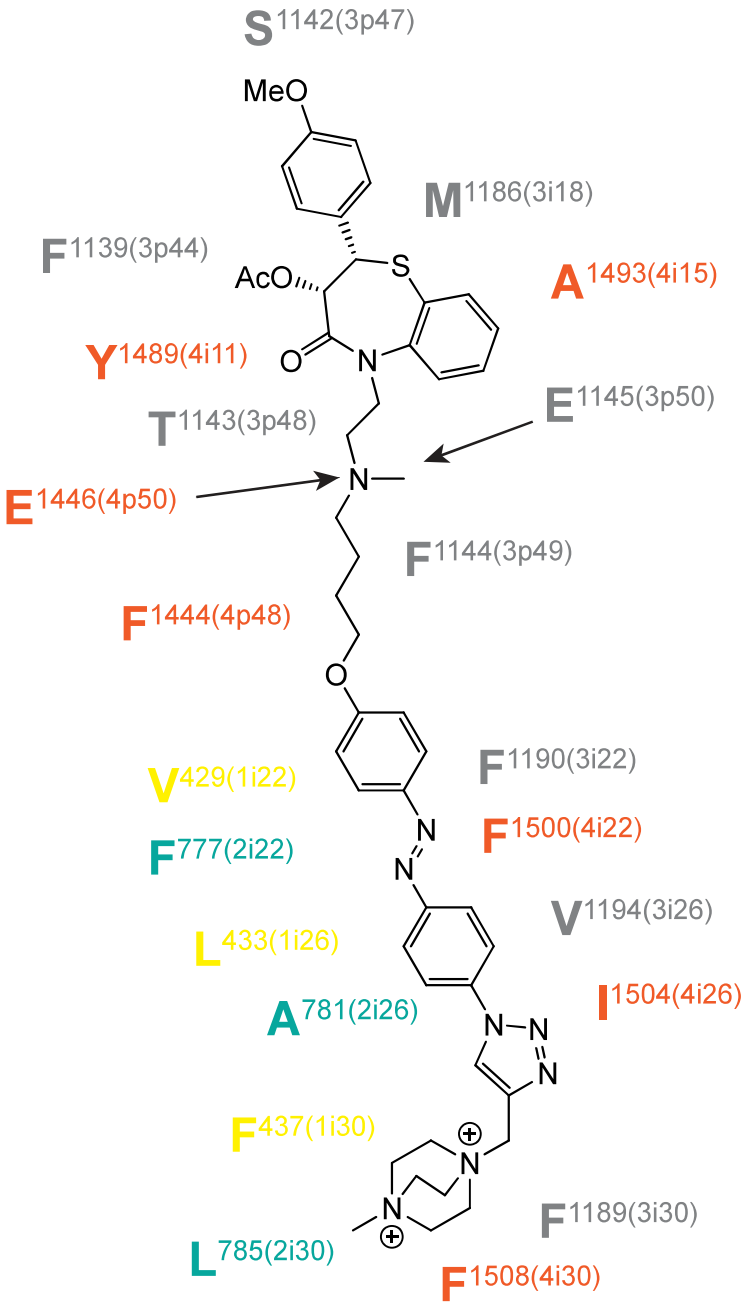

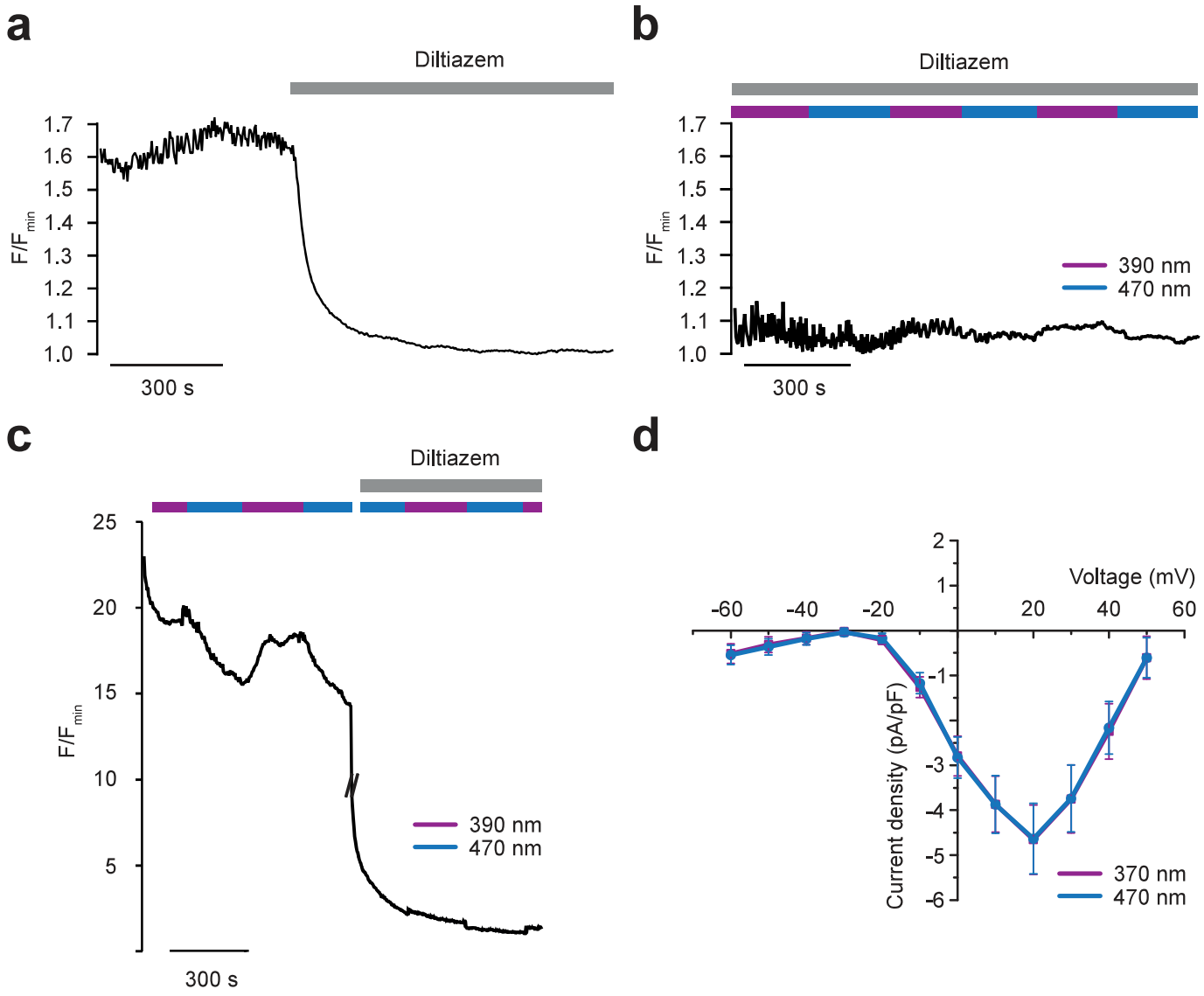
a
Diltiazem
1.7
1.6
1.5
1.4
1.3
1.2
1.1
1.0
F/F min
300 s
b
Diltiazem
1.7
1.6
1.5
1.4
1.3
1.2
1.1
1.0
F/F min
390 nm
470 nm
300 s
c
Diltiazem
25
20
15
10
5
F/F min
390 nm
470 nm
300 s
d
2
1
-1
-3
-4
-5
-6
-60
-40
-20
20
40
60
Voltage (mV)
Current density (pA/pF)
370 nm
470 nm

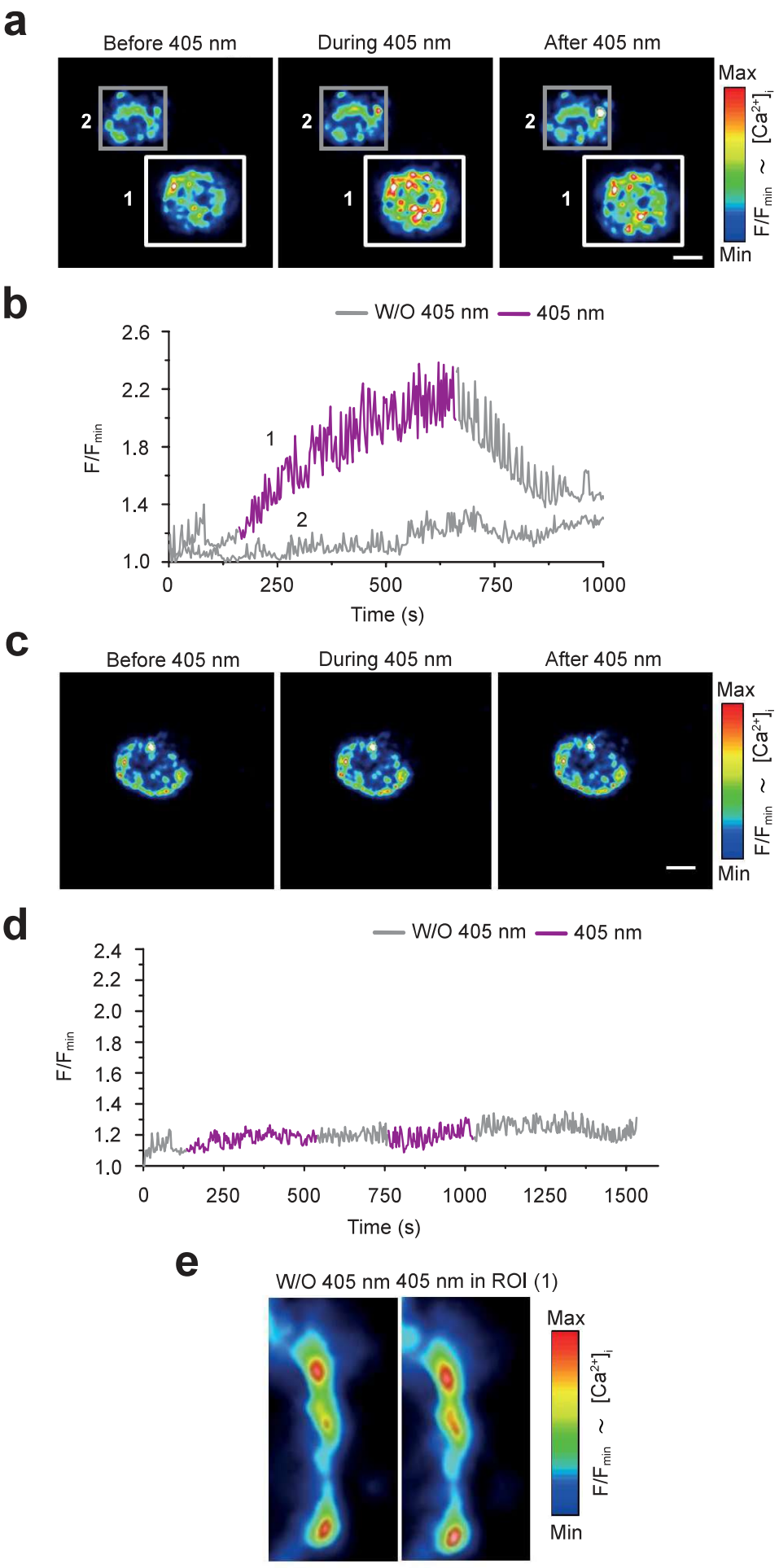
a
Before 405 nm
During 405 nm
After 405 nm
2
1
Max
Min
[Ca2+]i ~ F/Fmin
b
W/O 405 nm
405 nm
F/Fmin
Time (s)
c
Before 405 nm
During 405 nm
After 405 nm
Max
Min
[Ca2+]i ~ F/Fmin
d
W/O 405 nm
405 nm
F/Fmin
Time (s)
e
W/O 405 nm 405 nm in ROI (1)
Max
Min
[Ca2+]i ~ F/Fmin

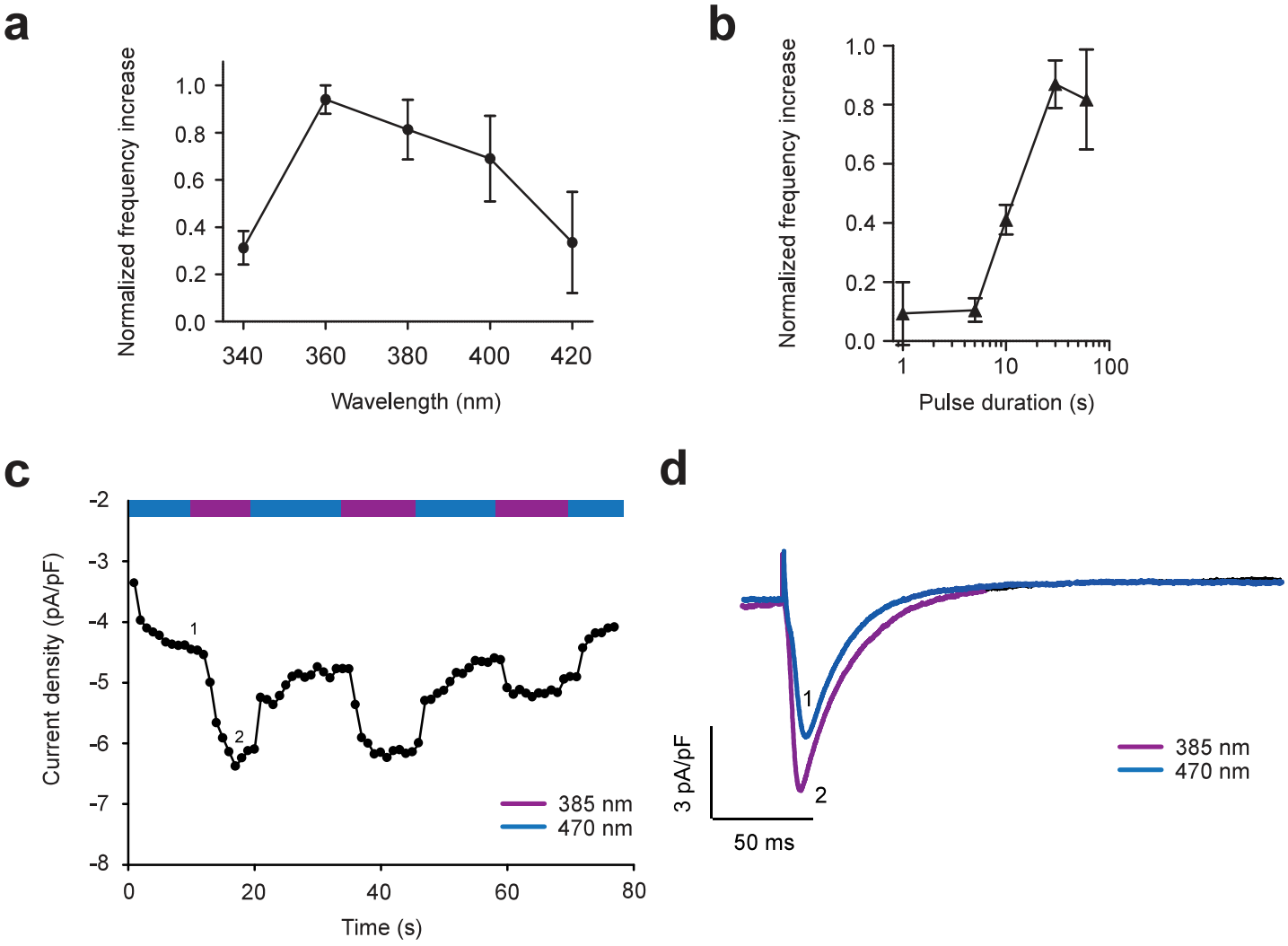
a
Normalized frequency increase
1.0
0.8
0.6
0.4
0.2
0.0
340
360
380
400
420
Wavelength (nm)
b
Normalized frequency increase
1.0
0.8
0.6
0.4
0.2
0.0
1
10
100
Pulse duration (s)
c
Current density (pA/pF)
-2
-3
-4
-5
-6
-7
-8
1
2
385 nm
470 nm
0
20
40
60
80
Time (s)
d
1
2
3 pA/pF
50 ms
385 nm
470 nm

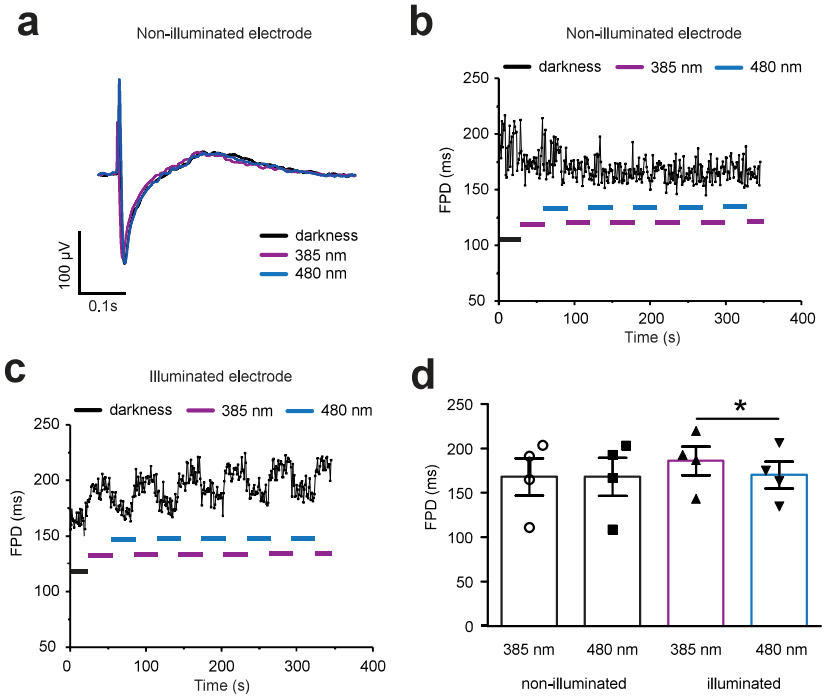
a
Non-illuminated electrode
darkness
385 nm
480 nm
100 µV
0.1s
b
Non-illuminated electrode
darkness
385 nm
480 nm
FPD (ms)
Time (s)
c
Illuminated electrode
darkness
385 nm
480 nm
FPD (ms)
Time (s)
d
FPD (ms)
*
385 nm
480 nm
385 nm
480 nm
non-illuminated
illuminated

a


150 ms
70 ms
762 ms
dark loop
355 nm
380 nm
3 ms
15 ms

b

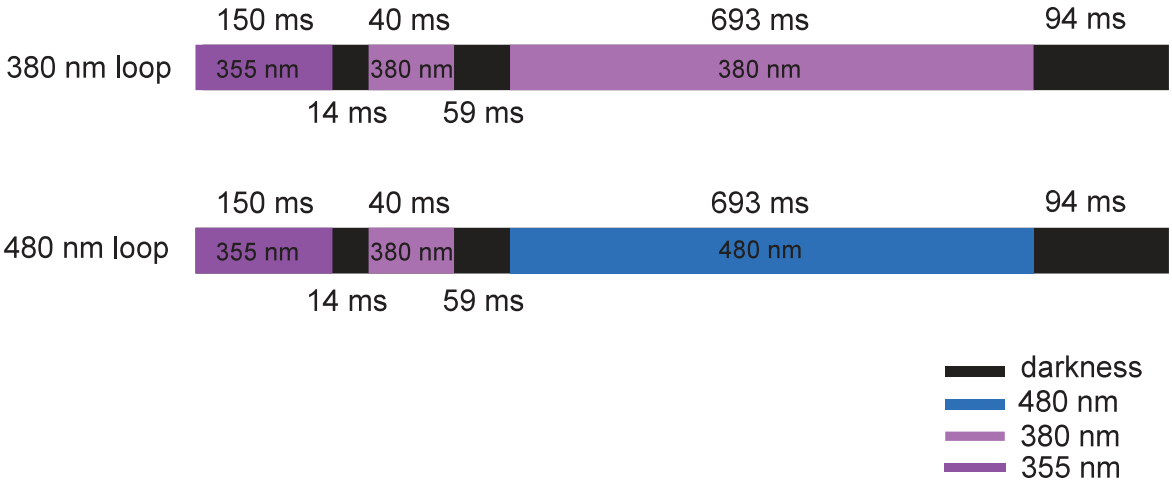
150 ms
40 ms
693 ms
94 ms
380 nm loop
355 nm
380 nm
380 nm
14 ms
59 ms
150 ms
40 ms
693 ms
94 ms
480 nm loop
355 nm
380 nm
480 nm
14 ms
59 ms
darkness
480 nm
380 nm
355 nm

Supplementary Table 1. Sequence alignment and benzothiazepine-sensing residues

Channel	Segment	# [a]	Sequence [b,c]
			p40 p50
			| |
Na_vAb	P	1159	WFGLGESF YTLFQVMTLE SWSMGIV
$Ca_v1.2$	IP	375	FDNFAFAM LTVFQCITME GWTDVLY
	IIP	719	FDNFPQSL LTVFQILTGE DWNSVMY
	IIIP	1128	FDNVLAAM MALFTVST**FE** GWPELLY
	IVP	1429	FQTFPQAV LLLFRCATG**E** AWQDIML
			i10 i20 i30
			| | |
Na_vAb	S6	1193	YAWVFFIPF IFVVFFVMIN LYVAIIVDAMAI
$Ca_v1.2$	IS6	410	LPWVYFVSL VIFGSFFVLN LVLGVLSGEFSK
	IIS6	758	LVCIYFIIL FICGNYILLN VFLAIAVDNLAD
	IIIS6	1171	EISIFF**I**IY **I**II**I**AFF**M**MN I**FV**GFVIVTFQE
	IVS6	1481	FAVFYF**I**SF **YM**LC**A**FL**I**IN LFVAVIMDNFDY

[a] Residue numbers in the $Ca_v1.2$ channel are given according UniProtKB - P15381 (CCAC_RABIT) and in the Na_vAb channel according to X-ray structures (PDB codes 5VB8, 5VB2).

[b] Labels, which are universal for P-loop channels [1], are shown above respective sequences.

[c] Experimentally determined benzothiazepine-sensing residues [2-4] are bold-typed and underlined.

Supplementary Table 2. Interaction energy of *trans*- and *cis*-FHU-779 with the $Ca_v1.2$ model partitioned by the channel residues [a]

P-loops	Energy, kcal/mol		S6	Energy, kcal/mol		S6	Energy, kcal/mol	
	trans-	*cis*-	*i11-i22*	*trans*-	*cis*-	*i23-i30*	*trans*-	*cis*-
$F^{1139(3p44)}$	-0.70	-2.98	$I^{1179(3i11)}$	-1.11	-1.16	$L^{778(2i23)}$	-0.58	
$S^{1142(3p47)}$	-1.97	-1.17	$Y^{1489(4i11)}$	-3.48	-2.20	$L^{1191(3i23)}$	-0.9	
$A^{1443(4p47)}$	-0.68	-2.39						
$T^{1143(3p48)}$	-2.37	-0.73	$I^{1180(3i12)}$		-0.53	$L^{433(1i26)}$	-3.05	
$T^{1444(4p48)}$	-3.11	-2.72	$M^{1490(4i12)}$	-1.19	-1.19	$A^{781(2i26)}$	-1.28	
$M^{391(1p49)}$	-1.03	-0.75				$V^{1194(3i26)}$	-1.08	
$F^{1144(3p49)}$	-2.22	-2.57	$I^{1182(3i14)}$	-1.12	-0.88	$I^{1504(4i26)}$	-1.16	
$E^{1145(3p50)}$	-0.90	-0.70						
$E^{1446(4p50)}$	-0.73	-0.67	$A^{1493(4i15)}$	-3.13	-1.75	$F^{437(1i30)}$	-1.62	
						$L^{785(2i30)}$	-1.13	
			$F^{1494(4i16)}$	-0.80		$F^{1198(3i30)}$	-1.45	
						$F^{1508(4i30)}$	-1.52	
			$F^{1185(3i17)}$	-0.52	-0.72			
			$V^{425(1i18)}$		-0.75			
			$L^{773(2i18)}$		-2.21			
			$M^{1186(3i18)}$	-2.22	-3.87			
			$I^{1496(4i18)}$	-0.93				
			$L^{426(1i19)}$	-1.21	-1.77			
			$L^{774(2i19)}$		-1.28			
			$M^{1187(3i19)}$	-0.80				
			$I^{1497(4i19)}$	-1.44				
			$V^{429(1i22)}$	-2.04	-1.13			
			$F^{777(2i22)}$	-0.61	-6.40			
			$F^{1190(3i22)}$	-3.65	-3.26			
			$F^{1500(4i22)}$	-3.55	-2.68			
Total	-14.91	-18.26	Total	-28.55	-35.14	Total	-15.90	0.00
			***trans*-FHU-779 Total**	**-58.73**		***cis*-FHU-779 Total**	**-53.40**	

Residues are designated by their genuine numbers in the rabbit $Ca_v1.2$ channel and bracketed universal labels (see **Supplementary Table 1**). Residues, for which the absolute value of their energy contribution to the ligand-channel interaction energy is less than 0.5 kcal/mol are not shown, but their energy contributions are included in the total energies. Residues whose mutations are known to affect action of benzothiazepines (**Supplementary Table 1**) are underlined.

Figure 1 | Design and characterization of the light-regulated diltiazem derivative FHU-779.

(**a**,**b**) Chemical structures of (**a**) diltiazem and (**b**) its photoswitchable derivative FHU-779. Thermally stable *trans*-FHU-779 can be isomerized to its *cis*-state using 385 nm irradiation, while 470 nm irradiation or thermal relaxation (k_BT) reverses the process. (**c**) The UV-Vis absorption spectra of FHU-779 under continuous irradiation at 380 nm, 480 nm or without additional illumination (dark). (**d-g**) Whole-cell patch clamp recordings of $Ca_v1.2$ Ba^{2+} currents in the presence of FHU-779 (25 µM) under 385 nm or 470 nm irradiation. $Ca_v1.2$ channels were heterologously expressed in HEK293T cells together with the β_3 and $\alpha_2\delta_1$ auxiliary subunits. (**d**) I-V relationship of peak currents under 385 nm or 470 nm illumination. Voltage dependent currents were elicited by stepping from –70 mV to +80 mV in 10 mV increments at 1 Hz for 100 ms. Indicated color code applies also for (**e**) and (**f**). (**e**) A representative single current trace demonstrates reversible light-dependent block of $Ca_v1.2$ by FHU-779 (25 µM). Displayed are the last triggered current-responses of 16 depolarizations under 385 nm and 470 nm irradiation, respectively. Currents were triggered by stepping from a holding potential of −70 mV to +30 mV at 1 Hz for 100 ms. Parallel lines represent time gap between currents. (**f**) Peak $Ca_v1.2$ Ba^+ currents under 385 nm and 470 nm irradiation over multiple cycles. (**g**) Quantification of photoswitching induced by extracellularly or internally applied FHU-779 (25 µM and 100 µM, respectively). Statistical evaluation by one way ANOVA test, $*p < 0.05$, $**p < 0.01$, $***p < 0.001$ (definition of photoswitching see online methods).

Figure 2 | FHU-779 enables optical control of LTCC conductance. (**a**,**b**) Ratiometric Ca^{2+} imaging of Fura-2- loaded HEK293T cells expressing $Ca_v1.2\Delta1671$, β_3, $\alpha_2\delta_1$ and TRAAK-GFP constructs in the presence of FHU-779. Cells were depolarized by K^+ (60 mM) to activate LTCCs. (**a**) Representative Ca^{2+} signals in a single transfected HEK293T cell under alternating 380 nm and 480 nm illumination (40 µM FHU-779). (**b**) Dose-response relationships of *trans*- and *cis*-FHU-779 determined by ratiometric Ca^{2+} imaging (see **Supplementary Fig. 3** and online methods). (**c,d**) The pore domain-model of the open L-type calcium channel with compound FHU-779 bound in the *trans*- (**c**) and *cis*- (**d**) conformations. The channel repeats I, II and IV are colored by yellow, magenta and cyan, respectively. For clarity, repeat III is not shown.

Figure 3 | FHU-779 allows photoswitching of LTCC in pancreatic β cells, cardiomyocytes and mouse hearts. (**a**) Reversible optical control of cytosolic Ca^{2+} levels measured by intensity-based Ca^{2+} imaging in mouse pancreatic islets using FHU-779 (35 μM). Representative Ca^{2+} signals from four islets (grey) imaged simultaneously (F/F_{min} represents fluorescence/minimal fluorescence in respective trace). The black line represents the mean. (**b**) Whole-cell patch clamp experiments in dissociated β cells. Displayed as the I-V relationship in the presence of FHU-779 (35 μM, n = 7 cells from 3 animals) under 370 nm and 470 nm irradiation. In all experiments, tolbutamide (200 μM) was added to block K_{ATP} channels and maintain LTCCs in the open state. (**c**) Insulin secretion under control conditions (11 mM glucose + 200 μM tolbutamide) and following application of either diltiazem (50 μM), *trans*-FHU-779 or *cis*-FHU-779 (35 μM) (n = 4 animals, circles represent individual data points). Statistical evaluation by one way ANOVA followed by Dunnett's multiple comparison test, $*p < 0.05$, $**p < 0.01$. (**d-f**) Ca^{2+} imaging of FHU-779 block release in single **β** cells residing within intact pancreatic islets. (**d**) Representative image before and during targeted irradiation of ROI (1) with 405 nm light (photoactivated ROI, white solid line (1); control ROI, grey solid line (2); scale bar = 50 μm; representative images, n = 7 islets from 3 animals). (**e**) Close up of photoactivated ROI (1) before and during 405 nm irradiation (colored map applies to **d** and **e**, W/O represents without). (**f**) Time course of F/F_{min}, before and during block release of representative ROIs (1 and 2) (n = 7 islets from 3 animals). (**g**,**h**) Heart rate modulation by FHU-779 (25 μM) in intact mouse hearts. (**g**) In the presence of FHU-779, 480 nm illumination of the right atrium decreased the spontaneous beating rate of a representative single heart. 380 nm reversed this effect. (**h**) Quantification of heart rate change induced by 380 nm light relative to 480 nm illumination before FHU-779 (W/O) and in the presence of FHU-779 (n = 4 hearts, two tailed, paired student t-test, $*p = 0.0375$). (**i**) Overlay of representative field potential (FP) signals of a monolayer Cor4U cardiomyocytes incubated with FHU-779 (10 μM). One electrode was in the illuminated region (**i**) of the MEA and the second electrode was in the non-illuminated area (**Supplementary Fig. 9**). The FP duration in (**i**) was determined to be 170.4 ± 14.8, 186.3 ± 15.9 ms for 480 nm and 385 nm, respectively (n = 4, paired t-test *p = 0.0159).